



Relationships among physical properties as indicators of high temperature deformation or post-shock thermal annealing in ordinary chondrites

Jon M. Friedrich^{a,b,*}, Alex Ruzicka^c, Robert J. Macke^f, James O. Thostenson^{d,2},
Rebecca A. Rudolph^{d,1}, Mark L. Rivers^e, Denton S. Ebel^{b,g,h}

^a Department of Chemistry, Fordham University, Bronx, NY 10458, USA

^b Department of Earth and Planetary Sciences, American Museum of Natural History, New York, NY 10024, USA

^c Cascadia Meteorite Laboratory, Portland State University, Department of Geology, Portland, OR 97207-0751, USA

^d Microscopy and Imaging Facility, American Museum of Natural History, New York, NY 10024, USA

^e Center for Advanced Radiation Sources, University of Chicago, Argonne, IL 60439, USA

^f Vatican Observatory, V-00120 Vatican City-State

^g Lamont-Doherty Earth Observatory, Columbia University, Palisades, New York 10964, USA

^h Graduate Center of the City University of New York, New York 10016, USA

Received 14 May 2016; accepted in revised form 31 December 2016; available online 11 January 2017

Abstract

Collisions and attendant shock compaction must have been important for the accretion and lithification of planetesimals, including the parent bodies of chondrites, but the conditions under which these occurred are not well constrained. A simple model for the compaction of chondrites predicts that shock intensity as recorded by shock stage should be related to porosity and grain fabric. To test this model, we studied sixteen ordinary chondrites of different groups (H, L, LL) using X-ray computed microtomography (μ CT) to measure porosity and metal fabric, ideal gas pycnometry and 3D laser scanning to determine porosity, and optical microscopy (OM) to determine shock stage. These included a subsample of six chondrites previously studied using transmission electron microscopy (TEM) to characterize microstructures in olivine. Combining with previous data, results support the simple model in general, but not for chondrites with low shock-porosity-foliation (low-SPF chondrites). These include Kernouvé (H6), Portales Valley (H6/7), Butsura (H6), Park (L6), GRO 85209 (L6), Estacado (H6), MIL 99301 (LL6), Spade (H6), and Queen's Mercy (H6), among others. The data for these meteorites are best explained by high ambient heat during or after shock. Low-SPF chondrites tend to have older $^{40}\text{Ar}/^{39}\text{Ar}$ ages ($\sim 4435\text{--}4526$ Ma) than other, non-low-SPF type 6 chondrites in this study. We conclude that the H, L, and LL asteroids all were shock-compacted at an early stage while warm, with collisions occurring during metamorphic heating of the parent bodies. Results ultimately bear on whether chondrite parent bodies have internal structures more akin to a metamorphosed onion shell or metamorphosed rubble pile, and on the nature of accretion and lithification processes for planetesimals.

© 2017 Elsevier Ltd. All rights reserved.

Keywords: Chondrites; Shock; Compaction; Porosity; Foliation; Asteroids; Annealing

* Corresponding author at: Department of Chemistry, Fordham University, Bronx, NY 10458, USA. Fax: +1 718 817 4432.

E-mail address: friedrich@fordham.edu (J.M. Friedrich).

¹ Present address: COMET Technologies USA, 100 Trap Falls Road Extension, Shelton, CT 06484, USA.

² Present address: Shared Materials Instrumentation Facility, Duke University, Box 90271, Durham, NC 27708, USA.

1. INTRODUCTION

Collisions were crucially important for the compaction of asteroidal-sized bodies, including those from which ordinary chondrites were derived. Although endogenous radiogenic (^{26}Al decay) heating alone would have resulted in some sintering (Henke et al., 2012), the parent bodies would have retained significant amounts of ancient porosity following accretion, owing to their small diameters. Lithostatic overpressure alone in a $\sim 100\text{--}300$ km body is completely insufficient for the reduction of remnant accretionary porosity (see Friedrich et al., 2014a for a discussion). It has been shown by observation and experiment that high velocity impact deformation alters the physical properties of materials in two ways: by reducing porosity, and by introducing foliation, both as a result of compaction (Cain et al., 1986; Nakamura et al., 1995, 2000; Gattacceca et al., 2005; Hirata et al., 2008; Friedrich et al., 2008a,b, 2013, 2014b). During a collision on a high porosity (e.g. $>20\text{--}25\%$) body, porosity is reduced, but in low ($\leq 2\text{--}3\%$) porosity bodies, shock produces brittle cracking of silicates which actually reintroduce porosity to a rock. Approximately $5\text{--}7\%$ porosity can be reintroduced by such microcracking (Consolmagno et al., 2008). Thus, the structure of the porosity in a chondrite is as important as the quantity of porosity for deciphering a chondrite's impact history. Foliation, or planar preferred grain orientations, in ordi-

nary chondrites has been observed and the strength of foliation correlates with increasing shock intensity recorded in a rock (Sneyd et al., 1988; Gattacceca et al., 2005; Friedrich et al., 2008a, 2014b). All of this leads to a simple model in which shock intensity and metal shape foliation is inversely related to porosity (Fig. 1).

Separating a chondrite's history into discrete accretionary, thermal metamorphic, and impact episodes is convenient, but the reality is much more complex. Ruzicka et al. (2015a) examined olivine microstructures by transmission electron microscopy (TEM) and optical microscopy (OM). They concluded that some chondrites experienced significant post-shock annealing (Ruzicka et al., 2015a), deformation while hot (Ruzicka et al., 2015a; Ashworth et al., 1977), or both (Ruzicka et al., 2015a), consistent with other evidence for high-temperature deformation (Friedrich et al., 2013; Scott et al., 2014; Friedrich et al., 2014a) and post-shock annealing (Rubin, 2002; Rubin and Jones, 2003; Rubin, 2004; Friedrich et al., 2014a). $^{40}\text{Ar}/^{39}\text{Ar}$ ages in many of these chondrites date to the metamorphic era of ordinary chondrite history (e.g., Swindle et al., 2014). In reality, decoupling thermal metamorphism and impact may not be fully realistic.

In this work, we test a simple model (Fig. 1) and reexamine the effects of shock compression on porosity and foliation in ordinary chondrites in light of growing evidence for complex relationships between impacts and thermal pro-

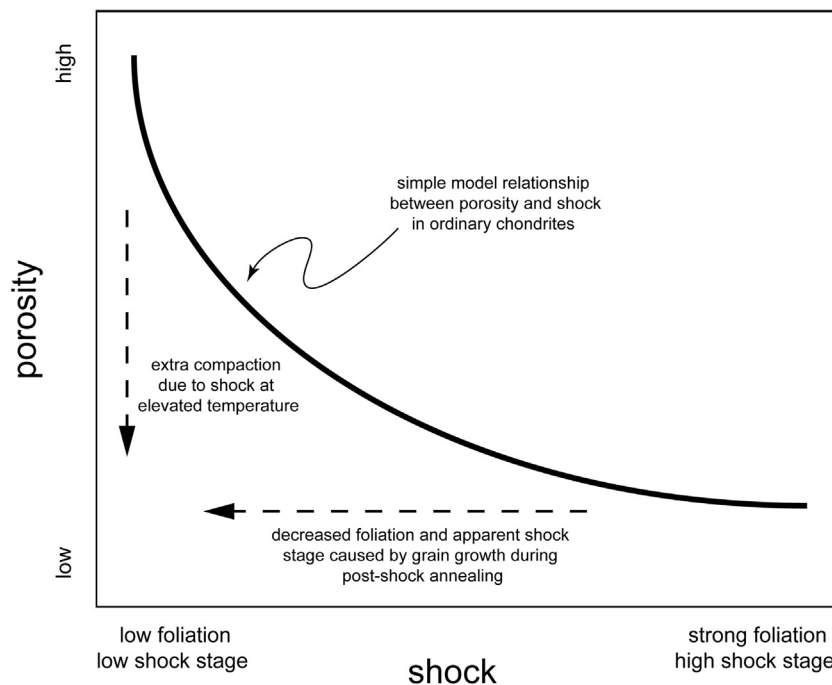


Fig. 1. Schematic diagram showing the expected relationship between shock stage, porosity, and metal grain foliation as a result of shock compaction. For the simple model trend (approximated by solid curve), stronger shocks decrease porosity and increase metal foliation. Increasing shock will reduce intergranular porosity until it is removed, except that additional shock will introduce intragranular microcracks, so porosity will never reach 0%. Even weak shocks might be capable of considerably reducing porosity, so porosity could decrease rapidly at low shock stage for slightly stronger shocks. The dashed vertical arrow represents a path for extra compaction caused by shock-related deformation of material already at elevated temperatures. The dashed horizontal arrow represents a path for apparent decreased foliation caused by grain growth and for lower shock stage by healing of defects during post-shock thermal annealing. These processes can cause chondrites to shift off of the simple model trend for weaker and stronger shocks.

cesses in these meteorites. Porosity, foliation strength, and petrographic observations are used to interpret the thermal metamorphic-shock histories of a suite of sixteen ordinary chondrites, including some of which are inferred to have experienced either impact-related deformation at high temperatures or significant post-shock annealing. The latter chondrites could have formed in asteroidal bodies near the base of a crater or deeply buried within warm material. Our results have implications for parent body structures and processes.

2. SAMPLES AND METHODS

2.1. Samples

Sixteen equilibrated (type 6) ordinary chondrites were examined for this study. Samples are listed in [Table 1](#) with additional details shown in [Supplementary Materials Table SM-1](#). Six are either finds or Antarctic finds (Estacado, Morrow County, Park, Spade, GRO 85209 and MIL 99301) while the remainder are falls.

Seven chondrites were selected because of previous evidence that they were either post-shock-annealed or experienced shock-related deformation while at elevated temperatures. These include: (1) Saint-Séverin (LL6) ([Ashworth et al., 1977](#); [Leroux et al., 1996](#)); (2) Butsura (H6) ([Ashworth, 1981](#); [Scott et al., 2014](#)); (3) Portales Valley (H6/7) ([Kring et al., 1999](#); [Rubin, 2004](#); [Ruzicka et al., 2005](#); [Scott et al., 2014](#); [Ruzicka et al., 2015a](#)); (4) Miller Range 99301 (hereafter MIL 99301) (LL6) ([Rubin, 2002, 2004](#); [Friedrich et al., 2014a](#); [Ruzicka et al., 2015a](#)); (5) Kernouvé (H6) ([Rubin, 2004](#); [Friedrich et al. 2013](#); [Scott et al., 2014](#); [Ruzicka et al., 2015a](#)); (6) Spade (H6) ([Rubin and Jones, 2003](#); [Rubin, 2004](#)); and (7) Park (L6) ([Ruzicka et al., 2015a](#)).

Nine meteorites were selected for other reasons. These include chondrites that have a variety of shock stages according to the [Stöffler et al. \(1991\)](#) shock stage scheme, or a variety of $^{40}\text{Ar}/^{39}\text{Ar}$ ages that indicate impacts occurring at different times, or that have evidence for “cold deformation” which differs from the chondrites mentioned above. GRO 85209, Holbrook, Alfianello, Tenham, Leedey, Bruderheim, and Morrow County are all L6 chondrites but vary in shock stage (nominally S1S6). Three of these (Leedey, Bruderheim, and Morrow County) showed evidence that shock deformation was initiated at low temperatures and was followed by fast cooling ([Ruzicka et al., 2015a](#)). Four of the L6 chondrites have younger $^{40}\text{Ar}/^{39}\text{Ar}$ ages (Leedey ~ 3800 Ma; [Bogard et al., 1987](#); Alfianello ~ 1050 Ma; [Kunz et al., 1997](#); Bruderheim ~ 465 Ma; [Turner, 1969](#); Morrow County ~ 460 Ma; [Ruzicka et al., 2015b](#)), whereas Queen’s Mercy (H6) and Estacado (H6) have relatively old (~ 4435 – 4490 Ma) $^{40}\text{Ar}/^{39}\text{Ar}$ ages ([Turner et al., 1978](#); [Trieloff et al., 2003](#)). Multiple $^{40}\text{Ar}/^{39}\text{Ar}$ ages were obtained for Saint-Séverin (~ 4383 , ~ 4420 Ma; [Hohenberg et al., 1981](#)) and MIL 99301 (~ 4230 , ~ 4520 Ma; [Dixon et al., 2004](#)) suggesting more complex shock histories, but still dominated by older impacts.

2.2. Methods

μCT imaging was performed at two different facilities for this study. For some samples, the GE phoenix v|tome|x s240 μCT system at the AMNH was used. This system is an instrument employing polychromatic X-ray radiation generated by an X-ray tube. Other samples were imaged with monochromatic x-rays at beamline 13-BM-D at the GeoSoilEnviro Center for Advanced Radiation Sources (GSE-CARS) at the Advanced Photon Source (APS) of Argonne National Laboratory. Instrument-specific μCT analytical parameters and resolutions are listed in detail within [Table SM-1](#). Analytical resolutions ranged between 6 and 18 $\mu\text{m}/\text{voxel}$ (a voxel is a 3D volume element akin to a 2D pixel or picture element). These resolutions yield interpretable data and derived products that are comparable to data from all previous studies using the same methodology (e.g. [Friedrich et al., 2014b](#) and references therein).

The 3D method presented in [Friedrich et al. \(2008a\)](#) and elaborated on in [Friedrich et al. \(2013\)](#) was used to quantify the magnitude of foliation of the metal grains in each μCT volume. This method produces a numerical value for the strength factor, C ([Woodcock, 1977](#); [Woodcock and Naylor, 1983](#)). The higher the numerical strength factor, the more pronounced the common orientation of the metal grains and the greater the foliation.

For some of our samples, two distinct chips were examined with μCT . Leedey was examined in [Friedrich et al. \(2008a\)](#) and an additional sample was examined with μCT for this work ([Table 1](#)). Kernouvé was analyzed with μCT in duplicate for a previous study ([Friedrich et al., 2013](#)) and the two samples of MIL 99301 are the same samples that were reported on in [Friedrich et al. \(2014a\)](#); however, new data (foliation strength) are presented for MIL 99301. All of these duplicate data are included in [Table 1](#) to allow for the evaluation of inter-sample variation of foliation strength ([Section 3](#)).

Bulk porosity measurements of four samples (Morrow County, Park, Spade, Saint-Séverin) for this work were accomplished via a combination of ideal gas pycnometry and laser scanning. Ideal-gas pycnometry utilizing a Quantachrome Ultrapycnometer 1000 pressurized with N_2 gas, provided grain density (ρ_g) (cf. [Consolmagno et al., 2006](#); [Macke, 2010](#)). Using a NextEngine ScannerHD Pro laser scanner, computer shape models were produced for each sample, from which the bulk volume and density (ρ_b) were determined ([Macke et al., 2015](#)). Porosity was calculated from these two quantities: $P = 1 - (\rho_b/\rho_g)$. For four samples (Butsura, GRO 85209, Portales Valley, Queen’s Mercy; see [Tables 1 & SM-1](#)), porosity was quantified using the μCT -based methods described in [Friedrich and Rivers \(2013\)](#). [Friedrich and Rivers \(2013\)](#) demonstrated that high resolution (2.6 $\mu\text{m}/\text{voxel}$ edge, [Table SM-1](#)) μCT imaging and digital quantification of porosity yields completely comparable results to ideal gas pycnometry. Other porosity values were taken from the exhaustive [Macke \(2010\)](#) database (see [Tables 1 and 2](#)). In cases of ordinary chondrite finds, the model porosity was used, determined from the sample’s measured bulk density and the average grain den-

Table 1
Sample list, with physical, petrographic and age data.

Meteorite	Symbol	Group & type	Shock stage ¹	Weighted shock stage ²	Subgrain boundaries ³	Foliation strength factor (C)	Porosity (%) ⁴	Ar age (Ma) ⁵
Alfianello	Alf	L6	S5	4.18 ± 0.56 (131)		1.13	8.7	1050 ± 60
Bruderheim	Brd	L6	S4	3.78 ± 0.66 (136)		0.56	5.7	465 ± 30
Butsura	But	H6	S1*	1.63 ± 1.00 (54)		0.23	6.6 ± 2.0	4480 ± 30
Estacado	Est	H6	S1	1.26 ± 0.74 (35)	Yes	0.40	4.3	4435 ± 5
GRO 85209	GRO	L6	S1	n.a.		0.03	2.2 ± 0.7	
Holbrook	Hol	L6	S3*	2.38 ± 1.16 (144)		0.65	10.4	4400 ± 100
Kernouvé [†]	Krn	H6	S1	1.13 ± 0.55 (115)	Yes	0.04, 0.12	5.8	4463 ± 11
Leedey	Ldy	L6	S4	3.94 ± 0.54 (162)		0.51, 0.66 [‡]	9.1	3800 ± 100
MIL 99301	MIL	LL6	S1*	1.60 ± 1.30 (65)	Yes	0.07, 0.10	10.5	4230 ± 30, 4520 ± 80
Morrow County	MC	L6	S5	4.46 ± 0.56 (149)		0.58	2.6 ± 1.6	460 ± 10
Park	Prk	L6	S1	1.35 ± 0.72 (153)	(yes)	0.04	8.3 ± 4.7	4526 ± 5
Portales Valley [#]	PV	H6/7	S1	1.16 ± 0.37 (100)	Yes	0.16	0.5 ± 0.2	4477 ± 16
Queen's Mercy	QM	H6	S3*	2.56 ± 1.09 (57)		0.65	2.5 ± 0.8	4490 ± 30
Saint-Séverin	SS	LL6	S4*	3.25 ± 1.23 (247)		0.34	9.9 ± 1.6	4383 ± 10, 4420 ± 10
Spade	Spa	H6	S4*	2.39 ± 1.36 (97)	Yes	0.30	6.6 ± 2.6	
Tenham	Ten	L6	S5	4.26 ± 0.64 (169)		0.80	4.4 ± 0.7	

¹ Conventional shock stage this study except for Bruderheim, Leedey, MIL 99301, Morrow County, Park, and Portales Valley (Ruzicka et al., 2015a) and Kernouvé (Friedrich et al., 2013b). Asterisks (*) indicate chondrites with inhomogeneous shock effects (see Text and weighted shock stage column).

² Weighted or mean shock stage (± denotes standard deviation value, value in parentheses give number of grains), using the method of Jamsja and Ruzicka (2010) and Ruzicka et al. (2015a). n. a. = not available.

³ Optically visible subgrain boundaries in otherwise lightly deformed olivine grains. Some subgrains are present in Park but fewer than in other meteorites that have them.

⁴ See Text for data sources and discussion of errors.

⁵ ⁴⁰Ar/³⁹Ar ages (K–Ar age for Holbrook), data from literature including: Kunz et al. (1997)—Alfianello; Turner et al. (1966) and Turner (1969)—Bruderheim; Trierloff et al. (2003)—Estacado, Kernouvé; Turner et al. (1978)—Butsura, Kernouvé, Queen's Mercy; Geiss and Hess (1958)—Holbrook; Bogard et al. (1987)—Leedey; Dixon et al. (2004)—MIL 99301; Ruzicka et al. (2015b)—Morrow County, Park; Garrison and Bogard (2001)—Portales Valley; Hohenberg et al. (1981)—Saint-Séverin.

[†] Kernouvé data reproduced from Friedrich et al. (2013).

[‡] Second Leedey datum from this work, other from Friedrich et al. (2008a).

[#] Silicate (excluding coarse metal vein) portion only.

Table 2
Compilation of additional data.

Meteorite	Group & type	Foliation strength factor (C)	Shock stage	Porosity (%)	References
Akaba	L6	0.51	–	–	Friedrich et al. (2008a)
Apt	L6	0.69	S4	8.4	Friedrich et al. (2008a), Macke (2010)
Atemajac	L6	0.31	–	–	Friedrich et al. (2008a)
Bachmut	L6	0.72	S3	6.3	Friedrich et al. (2008a), Macke (2010)
Barratta	L4	0.43	S4	5.3	Friedrich et al. (2008a), Macke (2010)
Baszkówka	L5	0.20, 0.05	S1	19.0	Friedrich et al. (2008a), Friedrich et al. (2008b), Friedrich et al. (2014a)
Bath Furnace	L6	0.39	–	4.6	This work, Macke (2010)
Bjurböle	L/LL4	0.31, 0.32, 0.26, 0.29	S1	19.8	Friedrich et al. (2008a), Macke (2010), this work
Bluff	L5	0.68	S6	4.0	Friedrich et al. (2008a), Macke (2010)
Castine	L6	0.49, 0.44	–	–	Friedrich et al. (2008a)
Chelyabinsk	LL5	1.23	S4	6.0	Popova et al. (2013), Kohout et al. (2014)
De Nova	L6	0.52	S2	–	Friedrich et al. (2008a)
Duruma	L6	0.40	–	–	Friedrich et al. (2008a)
Ellerslie	L5	0.69	S4	–	Friedrich et al. (2008a)
Fremont Butte	L4	0.68	S6	–	Friedrich et al. (2008a)
Grant County	L6	0.19	S2	–	Friedrich et al. (2008a)
Harrison County	L6	0.40	S2	–	Friedrich et al. (2008a)
Kyushu	L6	0.85	S5	5.4	Friedrich et al. (2008a), Macke (2010)
L'Aigle	L6	0.40	S2	6.8	Friedrich et al. (2008a), Macke (2010)
Mason Gully	H5	0.24	S2	10.8	Dyl et al. (2016)
McKinney	L4	0.64	S6	2.8	Friedrich et al. (2008a), Macke (2010)
Middlesbrough	L6	0.41	–	–	Friedrich et al. (2008a)
Miller (AR)	H5	0.06	S1	20.0	Sasso et al. (2009), Friedrich et al. (2014a), this work
Moorleah	L6	0.46	S3	–	Friedrich et al. (2008a)
Mount Tazerzait	L5	0.07	S1	12.6	Sasso et al. (2009), Friedrich et al. (2014a), this work
Novato	L6	0.96, 1.08	S4	–	Jenniskens et al. (2014)
NWA 2380	LL5	0.12	S1	18.7	Sasso et al. (2009), Friedrich et al. (2014a), this work
NWA 7298 (lith. A)	H3.8	0.28	S2	–	Friedrich et al. (2014b)
NWA 7298 (lith. B)	H3.8	0.78	S3	–	Friedrich et al. (2014b)
NWA 7298 (lith. C)	H3.8	0.19	S1	–	Friedrich et al. (2014b)
Quenggouk	H4	0.32	–	15.1	This work, Macke (2010)
Sahara 98034	H5	0.05	S1	16.1	Sasso et al. (2009), Friedrich et al. (2014a), this work
Saratov	L4	0.32, 0.32, 0.27, 0.27, 0.39	S2	13.5	Friedrich et al. (2008a), Macke (2010), this work
Tennasilm	L4	0.33, 0.36	S3	10.7	Friedrich et al. (2008a), Macke (2010)
Tjerebon	L5	0.05	S1	9.8	Sasso et al. (2009), Friedrich et al. (2014a), this work
Utrecht	L6	0.31	S3	–	Friedrich et al. (2008a)

sity for typical falls of that type, rather than the measured porosity to compensate for any potential terrestrial alteration effects (see [Consolmagno et al., 2008](#)). Errors for porosity are reported only for those samples that were measured for this study (Table 1). This is because errors for most previous results from [Macke \(2010\)](#) are not directly comparable to our own since the previous results are generally the mean of several to many individual analyses. A direct comparison may be misleading. A typical error for porosity measurements is on the order of 5–25% relative, with the majority of our samples possessing errors of <10% (see [Macke, 2010](#)). Using the porosity errors for samples in this study (Table 1), the average of the errors is 0.82% absolute. This can be taken as a representative error

for porosity that reflects some combination of analytical precision and sample heterogeneity.

Optical microscopy (OM) of petrographic thin sections was used to determine the shock stage of each sample using the method of [Stöffler et al. \(1991\)](#). Conventional shock stage is determined by the highest shock stage shown by at least 25% of olivine grains measured ([Stöffler et al., 1991](#)). A mean shock stage (“weighted shock stage”) was also determined by averaging the inferred shock stages for a large number of (typically $N > 100$) olivine grains, following the procedure of [Jamsja and Ruzicka \(2010\)](#) and [Ruzicka et al. \(2015a\)](#). In cases where there is significant variation between grains, the conventional shock stage can be misleading in part owing to the 25% rule, and the

weighted shock stage can better represent the overall optical deformation of olivine. Moreover, large variations in grain shock stages also can allow the identification of breccias and multiple impacts. Finally, we searched for olivine grains with low strain (minimal extinction variations in cross-polarized light) but containing low-angle subgrain boundaries (sharp changes in misorientation across well-defined boundaries) which can be an optical manifestation of microstructural recovery and annealing (Ruzicka et al., 2015a).

3. RESULTS

Shock stage classifications are shown in Table 1, and histograms of shock stages for individual olivine grains within each chondrite are shown in Fig. 2. Shock stage data indicate that some meteorites are breccias composed of a wide mix of individual grain shock stages. This includes Holbrook (S1- thru S4-dominant), Saint-Séverin (diverse, but S2- thru S4-dominant), Spade (bimodal, S1/S2- and S4-dominant), and Butsura and MIL 99301 (S1-dominant

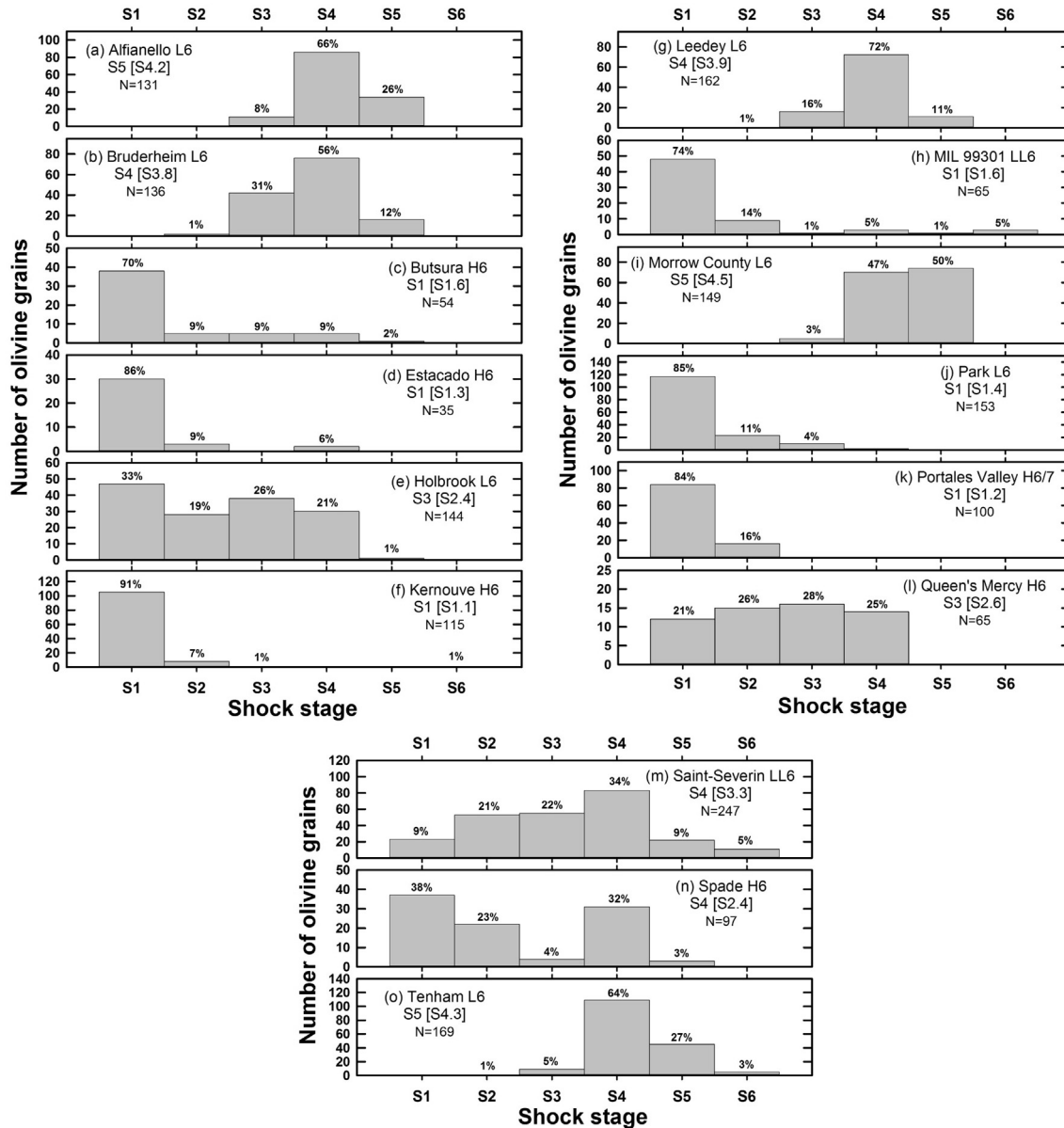


Fig. 2. Shock stage histograms for meteorites in this study based on optical microscopy data for olivine. Conventional shock stages are shown outside brackets, weighted shock stages given in brackets, and percentages of grains with different characteristics are given above bars. N = number of olivine grains. Values for grain percentages and weighted shock stages have been rounded. Queen's Mercy (part I) is designated as S3 based on non-rounded values.

but containing admixtures of more highly shocked material) (Fig. 2). Saint-Séverin also displays an obvious brecciated (clastic) texture. Such shock-heterogeneous chondrites are listed in Table 1 with asterisks next to their shock stages.

Other chondrites have more uniform shock stages. Good examples of these include Kernouvé and Portales Valley (predominantly S1), Leedeey (predominantly S4), and Tenham and Morrow County (predominantly S4 and S5) (Fig. 2).

Depending on whether they are heterogeneous or uniform in shock stages, chondrites thus have larger or smaller values of standard deviations in weighted shock stages (Table 1). An average of the standard deviations gives 0.42, which can be taken as a representative overall “error” in weighted shock stage for the meteorites in this study, caused primarily by sample heterogeneity.

Foliation strength factor, C , values for each sample are shown in Table 1. C values range from 0.03 (GRO 85209) to 1.13 (Alfanello), nearly spanning the range previously measured for ordinary chondrites (Table 2). Three of the meteorites examined in this study have multiple samples examined for petrofabrics with μ CT. This gives an opportunity for the examination of the variability that may be expected for different chips from the same stone. From the duplicate measurements, the largest absolute difference ($\Delta = 0.15$) can be found between the two Leedeey samples, where the determined C values are 0.51 and 0.66. The other samples in this study for which we have replicate data (Kernouvé, MIL 99301) give even more consistent results ($\Delta = 0.08$ and 0.03 respectively, Table 1). One literature compilation sample, Saratov, has had five replicate fabric analyses performed (see Table 2) and the standard deviation of the C value for them is 16% relative standard deviation (RSD). Taking all available data into account (Tables 1 and 2), the average of standard deviation values for C in a given meteorite is 0.027. This can be taken as a representative “error” for C , which largely reflects sample heterogeneity. Given that this “error” is much less than the total range in C among different meteorites, C values can be taken as representative of the stones as a whole.

Fig. 3 shows stereoplots for metal grain orientations in four chondrites that have different values of C (but similar porosity). The stereoplots show the direction of long axes of metal grains in three dimensions. With increasing value of C , the long axes of different grains become progressively concentrated in a plane (Fig. 3). This indicates that the C value can be taken as a measure of foliation strength in metal grains.

Fig. 4 shows the relationship between the degree of metal foliation and shock stage (both conventional and weighted). As previously demonstrated by Friedrich et al. (2008a) and others (Sneyd et al., 1988; Gattacceca et al., 2005), there is a correlation between foliation and the shock stage of a sample: with increasing shock stage, metal grains are more foliated. Spade and Saint-Séverin have perhaps a lower C value than may be expected when C is plotted against conventional shock stage (Fig. 4a), but appear less anomalous when C is plotted against weighted shock stage

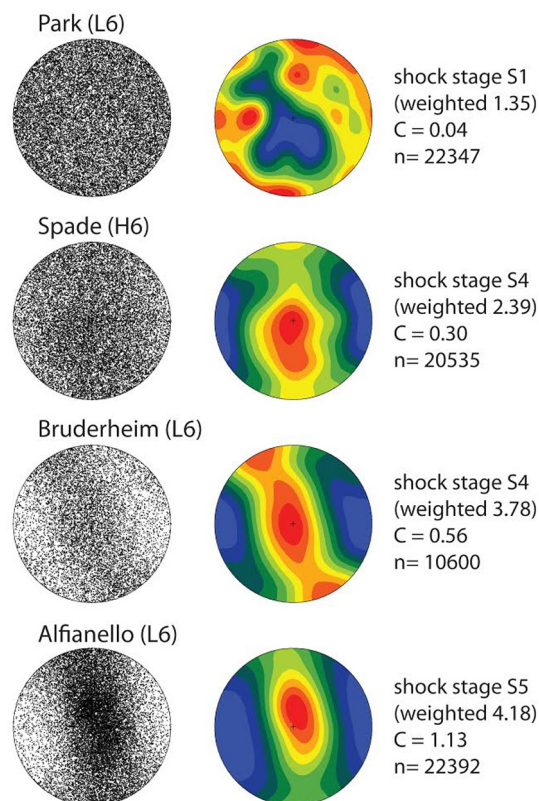


Fig. 3. Equal area stereographic projections (lower hemisphere) for metal grain shape orientations (long axes of metal grains) based on microtomography data for representative chondrites with different orientation strength factors, C . Individual grain data are at left and contoured data (red = higher concentrations, blue = lower concentrations of poles) at right. N = number of grains. (For interpretation of the references to colour in this figure legend, the reader is referred to the web version of this article.)

(Fig. 4b). Overall, these results conform to what is expected for the simple model (Fig. 1).

Porosity data are given in Tables 1 and 2. Porosities vary from ~ 0.5 to 9.9% for new measurements and between ~ 0.5 and 20.0% among all the ordinary chondrites. The relationship between porosity and shock stage (both conventional and weighted) is shown in Fig. 5. Consolmagno et al. (2008) demonstrated that there is a general trend of lower porosity with increased shock stage. However, they noted that while it is true to say that no high shock stage ordinary chondrites possess high porosity, some ordinary chondrites with low shock stages possess low porosity. This conclusion is consistent with the data obtained here. Namely, some chondrites with low shock stage (conventional and weighted) have relatively low porosities ($< 10\%$), similar to those of chondrites with high shock stages (Fig. 5). These results do not entirely conform to the simple model (Fig. 1).

Finally, the relationship between porosity and foliation strength C is shown in Fig. 6. Although there are no meteorites that have both high foliation strength and high porosities, and although the most porous chondrites have the lowest foliation strengths, there are also chondrites that

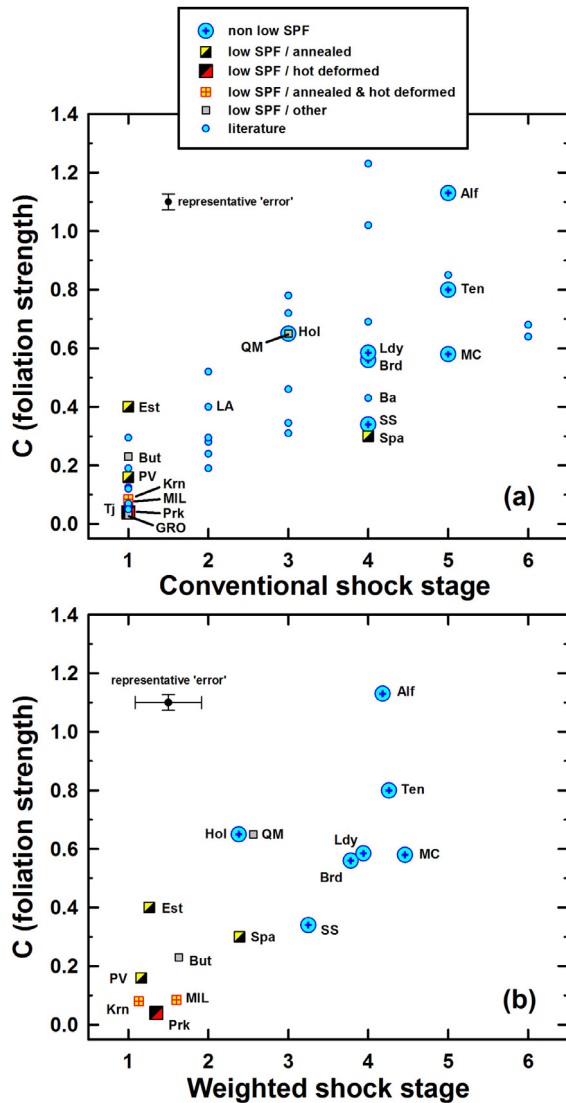


Fig. 4. Relationship between degree of preferred shape orientation of metal (embodied in the parameter C , foliation strength) and (a) conventional and (b) weighted shock stage. In cases where multiple C values were determined, an average is shown (except for the three lithologies for NWA 7298). Representative errors are based on an average of the standard deviation of C values (this study and literature) and an average of the standard deviation of weighted shock stage values (this study) for a given meteorite, with bar lengths = 1 standard deviation. Meteorite symbols are as in Table 1 and also: Tj = Tjerebon, LA = L'Aigle, and Ba = Barratta. Meteorites in this study are coded based on whether they are low-SPF (low shock-porosity-foliation) chondrites or not; see Text.

have both low porosity and low foliation strength (Fig. 6). These results again do not entirely conform to the simple model (Fig. 1).

4. DISCUSSION

4.1. Evidence for additional variables in shock deformation

Although the new data collected support the idea that shock deformation caused both a flattening of metal grains

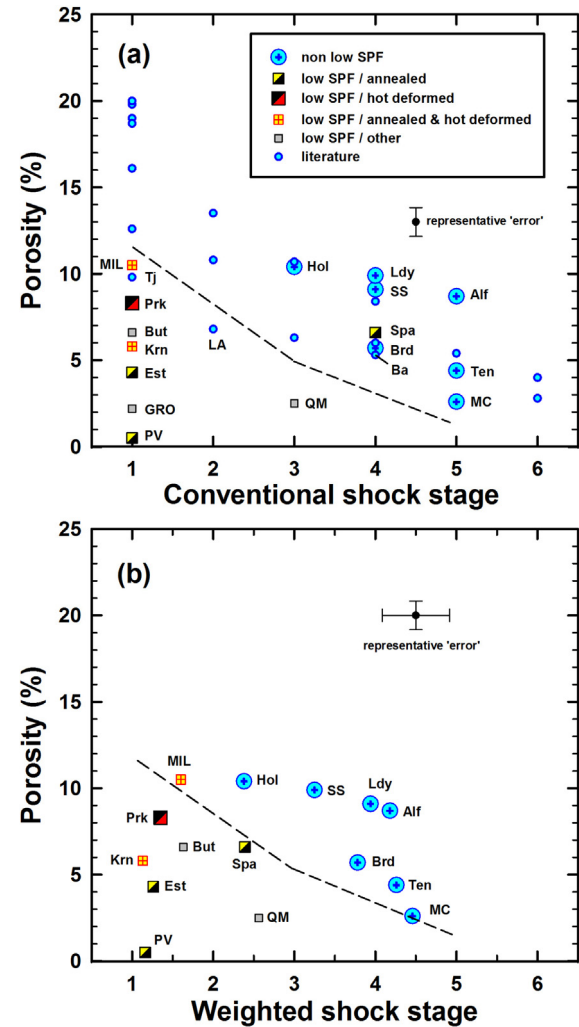


Fig. 5. Relationship between bulk porosity and (a) conventional and (b) weighted shock stage. In cases where multiple porosity values were determined, an average is shown. Representative errors are based on an average of the standard deviation of porosity values and an average of the standard deviation of weighted shock stage values for a given meteorite, with bar lengths = 1 standard deviation, utilizing data from this study. Meteorite symbols and designations are as in Table 1 and Fig. 4. The dashed line is a guideline dividing meteorites with low porosities and shock stages (below line) from others.

to create a foliation, as well as a collapse of pores to reduce overall porosity, there is evidence that the situation may be more complex than at first appears, with additional variables being important. Support for flattening is given by the general positive relationship between shock stage and orientation strength parameter C (Fig. 4), with the long axes of metal grains becoming concentrated in a plane (Fig. 3). Support for pore collapse is given by the general inverse relationship between porosity and shock stage (Fig. 5a). However, there is considerable scatter in both foliation and porosity for a given shock stage. Of particular note is the substantial variation in porosity shown by different S1 shock stage chondrites, ranging between ~0.5% and

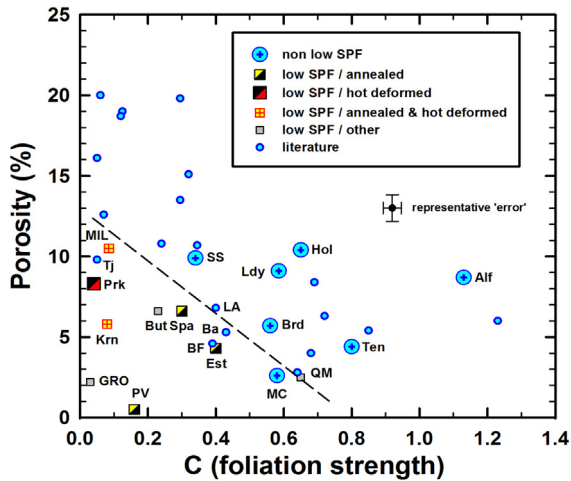


Fig. 6. Relationship between porosity and preferred shape orientation of metal grains (embodied in C , foliation strength). The dashed line is a guideline dividing meteorites with low porosities and foliations (below line) from others. Symbols, data, and abbreviations as described in Figs. 4 and 5, together with: BF = Bath Furnace.

20% (Fig. 5a). Higher porosity values could indicate the little shock compression expected by a weak shock, but there is no a priori reason to expect low porosity for some S1 chondrites. Moreover, shock compaction should produce an inverse relationship between metal foliation and porosity (Fig. 1), but there is again no a priori reason to expect the occurrence of chondrites with both low porosity and low metal foliation (Fig. 6). If a chondrite has experienced an impact intense enough to remove porosity, an intense foliation would be expected. Brecciation effects can complicate interpretations as materials with different shock stages can become mixed. However, Macke (2010) found little difference between porosities of brecciated and unbrecciated ordinary chondrites. Moreover, even with brecciation and mixing of materials with different shock stages, one might expect an inverse relationship between porosity and weighted shock stage. However, no such inverse relationship is evident (Fig. 5b).

Thus, there is evidence that the “simple model” for shock deformation (Fig. 1) is oversimplified, and that additional factors must be important. Two likely important variables not considered in simpler models are (1) the extent of post-shock annealing and (2) the ambient temperature of deformation. Both may be related to the amount of ambient heat in the parent body. Both could be explained by impact events occurring on parent bodies that were being metamorphosed.

Elevated post-shock temperatures can potentially anneal once-oriented metal grains in the target materials to destroy petrofabrics. There is evidence in H chondrites for increasing sphericity and size of metal grains with an increase in petrographic type (Guignard and Toplis, 2015), suggesting that petrofabrics will be destroyed if post-shock annealing conditions are similar to those involved in thermal metamorphism, as could be the case if shock occurred during thermal metamorphism. Moreover, there is mounting evi-

dence that post-shock annealing of chondrites can lessen apparent shock stages by decreasing optical strain in olivine (e.g., Rubin 2002, 2004; Rubin and Jones, 2003; Ruzicka et al., 2015a). Although it is conceivable that annealing could reduce porosity by allowing minerals to grow into pore spaces or by facilitating pore collapse, the latter process would be limited by lithostatic overburden pressures insufficient for complete pore collapse. Thus, post-shock annealing can potentially affect metal fabric and olivine shock stage, but porosity should be much less affected by annealing. The effect of post-shock annealing will be to shift chondrites to lower foliation and shock stage than they would otherwise have, i.e., to the left in Figs. 1, 5 and 6, and to the lower left in Fig. 4.

Besides annealing, pre-shock temperature could be an important variable. Shock loading experiments show that if pre-shock temperature is elevated, foliation increases and porosity decreases for a given shock pressure (Nakamura et al., 2000). Elevated pre-shock temperatures can affect how minerals respond to deformation, although optical deformation effects for olivine do not change drastically for shock experiments performed over a wide range of pre-heating temperatures (293–920 K) (Schmitt, 2000). Therefore, the effect of elevated pre-shock temperature will be to shift chondrites to lower porosities and higher foliations than they would otherwise have, i.e., downwards in Figs. 1 and 5, upwards in Fig. 4, and to the lower right in Fig. 6.

The role of brecciation and multiple impacts is discussed further in Section 4.4, but here it is useful to point out that these effects probably cannot explain chondrites with a combination of low shock stage, porosity, and foliation. In general, multiple impacts will cause extra compaction and a decrease in porosity (Nakamura et al., 2000), simulating the effect of fewer but stronger impacts. However, foliation mostly responds to the last strong impact (Friedrich et al., 2014b), so foliation might not change much unless subsequent impacts were stronger than what came before. Shock damage will be cumulative. In general, therefore, one would expect multiple shock events to have the effect of decreasing porosity, increasing shock stage somewhat, and having little effect on foliation in many cases. However, this does not readily explain chondrites that have low shock stage, low porosity, and low metal foliation. To explain such chondrites, some combination of post-shock annealing and elevated pre-shock temperature are more promising explanations.

4.2. Two groups of chondrites and their significance

Results suggest that chondrites can be subdivided into at least two groups based on their physical properties and shock stages. One group does not conform to the simple model for shock deformation and is here termed the “low-SPF group” (for low shock-porosity-foliation). The other group conforms to what is expected for the simple model and is here termed simply the “non-low-SPF group”. Table 3 identifies chondrites as belonging to one group or the other based on available data. In Figs. 5 and 6, dashed guidelines separate the two groups, with low-SPF

Table 3

Grouping of chondrites according to their physical properties and shock stages. Meteorites with asterisks indicate those in this study, and those in parentheses have borderline values and less certainly fit within the respective groups.

Chondrites with low shock stage & porosity	Chondrites with low porosity & metal foliation	Chondrites with low shock stage & porosity & metal foliation (low-SPF group)	Other chondrites (non-low-SPF group)
Butsura*	(Barratta)	Bath Furnace? ¹	Alfianello*
Estacado*	Bath Furnace	Butsura*	Bruderheim*
GRO 85209*	Butsura*	Estacado*	Holbrook*
Kernouvé*	Estacado*	GRO 85209*	Leedey*
L'Aigle	GRO 85209*	Kernouvé*	Morrow County*
(MIL 99301*)	Kernouvé*	(L'Aigle)	Saint-Séverin*
Park*	(L'Aigle)	(MIL 99301*)	Tenham*
Portales Valley*	(MIL 99301*)	Park*	+
Queen's Mercy*	(Morrow County)*	Portales Valley*	31 others (Table 2)
(Spade*)	Park*	(Queen's Mercy*)	
Tjerebon	Portales Valley*	Spade*	
	(Queen's Mercy*)	Tjerebon	
	Spade*		
	Tjerebon		

¹ No shock stage determination.

chondrites having relatively low porosity for a given shock stage (Fig. 5), and having both low porosity and low metal foliation (Fig. 6). The exact placement of the guidelines in these figures is somewhat arbitrary. However, as shown in Table 3 and Figs. 5 and 6, there is substantial overlap in groupings based on (1) low shock stage and low porosity, and (2) low porosity and low metal foliation. This suggests that low-SPF chondrites form a relatively coherent group, with different combinations of properties largely identifying the same group of meteorites. By extension, non-low-SPF chondrites (anything that is not in the low-SPF group) also form a relatively coherent group. However, there is some ambiguity for group assignments, especially for those chondrites that have intermediate shock stages, porosities, and metal foliations.

The best explanation for creating a low-SPF chondrite is some combination of post-shock annealing and elevated pre-shock temperature (Section 4.1). This inference is consistent with other data for these chondrites, as discussed in more detail in Section 4.3 and below.

Some chondrites assigned to the low-SPF group show especially good evidence for annealing or high-temperature deformation. These include Estacado, Kernouvé, MIL 99301, Portales Valley, Spade, and Park. All but Park have a significant number of optically visible subgrain boundaries in olivine that could signify post-shock annealing, and even Park has some of these subgrain boundaries (Table 1). In Kernouvé, MIL 99301, and Portales Valley, TEM evidence indeed suggests that subgrain boundaries were produced by annealing (Ruzicka et al., 2015a). In Kernouvé, MIL 99301, and Park, TEM evidence suggests that deformation occurred under conditions of elevated pre-shock temperature (Ruzicka et al., 2015a). Using the best available data, these various low-SPF chondrites are coded in Figs. 4–6 according to whether they are annealed (Estacado, Portales Valley, Spade), hot-deformed (Park), or both annealed and hot-deformed (Kernouvé, MIL 99301).

Other chondrites assigned to the low-SPF group include GRO 85209, Butsura, Tjerebon, and possibly Queen's Mercy and L'Aigle (Table 3). Currently it is not known for certain whether these chondrites were annealed or hot-deformed, so they are coded in Figs. 4–6 as “other low-SPF” chondrites, although there is some evidence for both annealing and hot deformation in Butsura (Section 4.3.5). Bath Furnace has relatively low porosity and metal foliation but no shock stage determination, so it is unclear whether it is a low-SPF chondrite (Table 3).

In contrast, many other meteorites belong to the non-low-SPF group (Table 3). This includes the L6 chondrites Alfianello, Bruderheim, Holbrook, Leedey, Morrow County, and Tenham. There is reason to suppose that they were shocked on a cold parent body. None show obvious subgrain boundaries that can be attributed to annealing. Prior TEM work (Ruzicka et al., 2015a and references therein) suggested that at least Bruderheim, Leedey, and Morrow County experienced relatively simple or idealized shock histories: their predominant shock deformation was initiated at low temperatures and was followed by fast cooling. Furthermore, these impacts occurred far later than the time thermal metamorphism was active on the parent asteroid and so must have occurred when the asteroids were cold. For instance, ⁴⁰Ar/³⁹Ar ages for Leedey (3800 ± 100 Ma) (Bogard et al., 1987), Bruderheim (465 ± 30 Ma) (Turner et al., 1966; Turner, 1969), and Morrow County (460 ± 10 Ma) (Ruzicka et al., 2015b) suggest late impact events on the L chondrite parent body, with the latter two ages corresponding to the inferred break-up event of the L asteroid (e.g., Swindle et al., 2014). Similarly, Alfianello (⁴⁰Ar/³⁹Ar age 1050 ± 60 Ma; Kunz et al., 1997) and Tenham are strongly shocked (S5) chondrites in which shock and related (re)heating episodes appear to have occurred in a post-metamorphic setting. Although the ⁴⁰Ar/³⁹Ar age of Holbrook potentially dates to a metamorphic era (4400 ± 100 Ma), it seems to be a non-low-SPF chondrite based on somewhat elevated values of shock

stage and foliation strength, and a porosity that is not overly low for the given shock stage and foliation (Figs. 5 and 6).

Barratta (L4) probably also belongs to the non-low-SPF group as it has a somewhat high conventional shock stage of S4, although it does have somewhat low porosity and metal foliation (Fig. 6). Saint-Séverin (LL6) likewise appears to belong to this group (Table 3), although it may have been shocked while warm (Ashworth et al., 1977).

4.3. Annealed or hot-deformed chondrites

We assign Kernouvé, Portales Valley, GRO 85209, Park, Butsura, Estacado, MIL 99301, Spade, and Queen's Mercy to the group of chondrites that exhibit a combination of relatively low shock stages, low porosities, and low metal foliations (low-SPF group, Table 3), which could reflect post-shock annealing or deformation while hot (Sections 4.1 and 4.2). In agreement with this, most of these chondrites, along with Saint-Séverin, were previously suggested based on various data to have been annealed following shock or deformed while warm (Section 2.1). The shock histories of these meteorites are discussed individually below.

4.3.1. Kernouvé

Kernouvé is an H6 chondrite with an S1 shock stage. The relatively low porosity of Kernouvé (5.8%) is in the form of intergranular voids rather than intragranular cracks (Friedrich et al., 2013). In Kernouvé the intergranular voids are likely the remains of incomplete compaction during impact, in contrast to intragranular cracks that are generally interpreted as being produced after full compaction and subsequent cracking of the brittle silicates (Consolmagno et al., 2008; Friedrich and Rivers, 2013). Despite such incomplete compaction, preferred orientation of the metal grains is minimal (Fig. 6).

Based on an old $^{40}\text{Ar}/^{39}\text{Ar}$ age and the presence of coarse metal veins that could have formed by shock melting, Rubin (2004) hypothesized that Kernouvé was impacted and then annealed during thermal metamorphism. Friedrich et al. (2013) came to a similar conclusion regarding the timing and nature of the impact-related compaction experienced by Kernouvé. As they found no significant collective orientation of metal grains they concluded that high metamorphic temperatures following compaction erased any common orientation of metal grains due to compaction. Furthermore, a coarse metal vein imaged in 3D by these authors was interpreted as showing evidence for formation by shear and subsequent grain growth during metamorphism. Scott et al. (2014) also suggested that Kernouvé could have been impacted during metamorphism of the H chondrite parent body. Their inferred metallographic cooling rate of 10 °C/Ma for Kernouvé is one of the lower values they obtained for H chondrites and suggests low-temperature annealing as a result of deep burial. Ruzicka et al. (2015a) inferred slow post-shock cooling for the meteorite at a higher temperature, sufficient to allow migration of dislocations in olivine into subgrain boundaries. These authors also found evidence for shock occurring at an

elevated temperature, but no evidence that Kernouvé was ever shocked above an S1 shock stage level.

Kernouvé thus appears to have been weakly shocked at high temperature during thermal metamorphism to form metal veins, and to have cooled slowly from metamorphic temperatures. The moderately low porosity (Figs. 5 and 6) suggests some pore collapse caused by only a weak or moderate shock pressure, perhaps aided by high temperatures. The very low foliation suggests considerable annealing to obliterate any early metal fabric and to modify the metal veins. Most likely Kernouvé formed and cooled in hot basement materials on the H-chondrite asteroid, and experienced at least some shock compaction while warm.

4.3.2. Portales Valley

Portales Valley is an H chondrite with distinctive coarse metal veins (Kring et al., 1999) and has the lowest measured porosity (0.5%) of any of the chondrites shown in Figs. 5 and 6. This porosity measurement only includes the silicate fraction and does not include the coarse metal vein material, so the low porosity value is even more striking as metal would be expected to have low porosity. Using the Stöffler et al. (1991) scheme, Portales Valley is clearly within the lowest shocked (S1) category based on olivine; however, the extensive metal veining in Portales Valley has been interpreted as being due to shock mobilization associated with impact cratering on the H chondrite asteroid (Kring et al., 1999; Rubin, 2004; Ruzicka et al., 2005). A fine Widmanstätten structure in coarse metal and cooling models for zoned taenite grains indicate that Portales Valley cooled slowly at low temperatures after impact (Kring et al., 1999; Ruzicka et al., 2005; Scott et al., 2014). Moreover, well-developed subgrain boundaries in olivine were interpreted as evidence of slow post-shock cooling at elevated temperatures (Ruzicka et al., 2015a). Unlike the situation for Kernouvé, the latter authors found evidence that olivine in Portales Valley was significantly deformed prior to annealing. Dislocation densities in vestigial heavily-deformed areas are comparable to that found in S4 to S5 chondrites, leading Ruzicka et al. (2015a) to conclude that the original olivine shock stage for Portales Valley prior to recovery could have been as high as S4 or S5, although the precise shock intensity was uncertain. The meteorite could have been close to peak metamorphic temperature at the time of impact (Ruzicka et al., 2005; Scott et al., 2014), a possibility that is consistent with (but not necessarily demanded by) olivine microstructural data (Ruzicka et al., 2015a). Thus, extensive annealing following possibly high-temperature deformation is suggested for Portales Valley.

Porosity and metal foliation data for Portales Valley are consistent with an important role for annealing and high-temperature deformation. The very low porosity of Portales Valley is consistent with a strong shock (\geq S4) occurring at high temperature to result in maximal pore collapse (Figs. 1 and 5). Annealing during slow post-shock cooling was likely responsible for producing both the low shock stage and low amount of metal foliation of the meteorite, involving both a significant decrease in apparent shock stage and a decrease in foliation strength (Figs. 1 and 4). For an initial

shock stage of S4 or S5 that was reduced to S1, the foliation strength could have been decreased dramatically (C from ~ 0.5 – 1.1 to ~ 0.15 , Fig. 4). All data support the idea that Portales Valley formed and cooled in warm basement materials on the H chondrite asteroid below an impact crater.

4.3.3. GRO 85209

GRO 85209 was included in our study as a representative of an L6 chondrite with an uncommon (for L chondrites) S1 shock stage. Our data indicate that GRO 85209 has both low porosity (2.2%) and also a near lack of foliation in the metal grains. In terms of shock stage, porosity, and metal foliation, GRO 85209 is similar to Kernouvé and Portales Valley (Figs. 4a, 5a, 6), and so could have formed in a similar manner, although on a different parent body (L instead of H). Although few other studies on GRO 85209 exist for comparison, we propose that based on the relationships among physical properties, GRO 85209 was likely annealed to a high degree after a substantial impact at elevated temperature that removed much of the porosity.

4.3.4. Park

As with GRO 85209, Park is an L6 chondrite with a low (for an L chondrite) S1 shock stage. OM data confirm the S1 designation (Table 1). Some subgrain boundaries in olivine are visible optically (Table 1), suggestive of annealing, but little evidence for post-shock annealing was noted with TEM (Ruzicka et al., 2015a). TEM observations of olivine microstructures showed that Park experienced mild deformation at high temperatures (Ruzicka et al., 2015a). Olivine microstructures for Park together with a precise $^{40}\text{Ar}/^{39}\text{Ar}$ age of 4528.8 ± 4.6 Ma (Ruzicka et al. 2015b) were interpreted to indicate early deformation followed by relatively rapid cooling, with Park impact-excavated to a shallower level of a warm parent body (Ruzicka et al., 2015a,b).

Park has moderately low porosity and a low degree of metal foliation (Figs. 5 and 6). The porosity in Park is dominated by intergranular porosity with few intragranular microcracks. On a porosity – shock stage plot (Fig. 5), the porosity of Park is more like that of a typical S2 or S3 chondrite, but based on OM and TEM data it does not seem likely that strain in olivine consistent with S2–S3 levels was obliterated by annealing to make an S1 level (Ruzicka et al., 2015a). Rather, the low porosity for Park can be explained by relatively weak (S1) high-temperature deformation promoting more compaction that would otherwise be the case for a cold target. The low degree of preferred metal orientation could be partly the result of a weak shock to begin with, but given that foliation is lower in Park than many other S1 chondrites (Figs. 4 and 6), it seems likely that post-shock annealing obliterated preferred orientation for metal. If so, post-shock cooling was not overly rapid, and Park may not have been excavated to the very surface of the parent body, but rather to a shallow, somewhat cooler level than in which it originally formed.

4.3.5. Butsura

Butsura (H6) is classified as shock stage S1. Ashworth (1981) found that although shock effects in Butsura were

inhomogeneous within the brecciated (Table 1) sample, there was evidence of some annealing of olivine after deformation. An ancient $^{40}\text{Ar}/^{39}\text{Ar}$ age for Butsura (4480 ± 30 Ma; Turner et al., 1978) suggests the shock-related deformation occurred during metamorphism, as a later shock event and the elevated thermal temperatures associated with it would have been recorded by the ^{40}Ar – ^{39}Ar system. Much like Kernouvé (Section 4.3.1), Butsura has a ~ 30 cm long millimeter-wide vein of metallic Fe–Ni (Hutchison, 2004). Such veins are nearly identical to those seen in Kernouvé, which were hypothesized to be due to pre- or syn-metamorphic impact-related deformation (Friedrich et al., 2013; Scott et al., 2014). Using metallographic techniques, Scott et al. (2014) found a relatively slow (10–100 °C/Myr) cooling rate for Butsura, which suggests deep burial within the parent body.

The 6.6% porosity contained in Butsura is lower than would be expected for an ordinary chondrite of S1 shock stage (Fig. 5) and could indicate that over half of the primordial porosity of Butsura was removed. However, this compaction is not reflected in terms of appreciably higher foliation strength (Fig. 6). The porosity structure of Butsura is identical to that seen in Kernouvé (see Friedrich et al., 2013): intergranular, due to incomplete compaction.

Thus, it appears that Butsura was shocked early, possibly at high temperature, and cooled slowly afterwards at depth in the H chondrite asteroid. The impact removed some porosity and somewhat oriented the metal grains. However, the deep burial and slow cooling annealed olivine deformation and partially removed preferred orientation in the metal grains. As with Kernouvé and Portales Valley, Butsura likely formed beneath an impact crater on the H chondrite parent body.

4.3.6. Estacado

Like Butsura, Estacado is an H6 chondrite. μCT investigation of the porosity shows the majority of the 4.3% porosity is intergranular, again suggesting incomplete compaction rather than porosity due to shock-induced microcracks within silicate grains. The metal foliation seen in Estacado is the highest known for an S1 chondrite (Fig. 4). This foliation strength is strong enough to be matched by chondrites of shock stage S2 or S3 (Fig. 4). Estacado possesses a porosity of only 4.3%, which is about one-third of what may be expected for a chondrite of S1 shock stage (Fig. 5a). If we were to consider only the porosity and degree of foliation of Estacado, a reasonable estimate for the shock stage would be S3 (Figs. 4 and 5). However, our S1 classification of Estacado's shock stage is corroborated with others' assessments (Rubin, 2004; Scott et al., 2014). Given the low shock stage and strong foliation for an S1 chondrite, compaction of materials that were already warm followed by post-shock annealing to lessen olivine deformation could explain the data. Annealing is supported by optical identification of subgrain boundaries in Estacado olivine (Table 1) similar to that produced by recovery. However, annealing could not have been overly extensive, for otherwise one would expect this to have destroyed metal foliation.

4.3.7. MIL 99301

MIL 99301 (LL6) has been extensively studied (Rubin, 2002, 2004; Friedrich et al., 2014a; Ruzicka et al., 2015a). Two Ar ages are recorded for the meteorite, ~4520 and ~4230 Ma (Dixon et al., 2004). Based on potential petrographic shock indicators, Rubin (2002, 2004) concluded that MIL 99301 was shocked to high (~S4) levels, and later annealed, possibly due to post-metamorphic impact heating. Friedrich et al. (2014a) examined MIL 99301, noted its substantial porosity in the form of intergranular voids, and suggested that impacts into materials that were already hot may have produced the relict shock indicators noted by Rubin (2002, 2004) and Friedrich et al. (2014a). Ruzicka et al. (2015a) found microstructural evidence in olivine both for high-temperature deformation and post-shock annealing. They suggested that MIL 99301 olivine could have experienced significant recovery, possibly lessening the shock stage from ~S2-S3 to S1.

Considering MIL 99301 in the context of this work, the porosity of the meteorite is somewhat intermediate between low-SPF and non-low-SPF S1 chondrites (Fig. 5a). The porosity is appropriate for what one would expect for S2 or S3 chondrites (Fig. 5), so shock of this intensity followed by annealing and recovery of olivine to S1 shock stage could explain both the porosity and olivine data. The foliation strength of MIL 99301 is at the low end of foliations known for ordinary chondrites, and lower than S2 and S3 as well as higher shock stage chondrites (Fig. 4). This suggests that metal foliation in MIL 99301 was largely eliminated by the same annealing event that affected olivine. Thus, MIL 99301 could have been shocked while warm and then annealed, with the latter process being especially important for olivine recovery and reducing metal foliation. Cooling likely occurred at depth in the warm LL parent asteroid. At a later stage, possibly at ~4230 Ma ago, a small proportion of more highly shocked material could have been incorporated into the MIL 99301 source area to account for its presence in the rock (Ruzicka et al., 2015a) (Table 1, Fig. 2h), but any later impacts evidently did not introduce much microcracking nor result in metal foliation.

4.3.8. Spade

Spade is an H6 chondrite. Rubin and Jones (2003) and Rubin (2004) shock-classified Spade and found a shock stage of S2, which differs from our own shock stage classification of S4. The latter is somewhat misleading, however, as the weighted shock stage for Spade is only 2.39 (Table 1), which is similar to the Rubin and Jones (2003) and Rubin (2004) conventional shock value. Our OM data suggest that Spade is actually an S1-S2, S4 bimodal breccia, with 38%, 23%, and 32% of olivine grains consistent with shock stages of S1, S2, and S4 respectively (Fig. 2n). These grains of different shock stages are intimately mixed. The previous investigators found that Spade was best described as an annealed impact melt breccia. The brecciated nature of Spade and how one designates conventional shock stage for such breccias likely accounts for the differences in classification between the investigations.

For Spade, porosity and metal foliation strength factor are both low compared to other chondrites, but not overly so (Fig. 6). Much of the porosity is in the form of microcracks. Spade also shows optical evidence for subgrain boundaries in olivine (Table 1), consistent with annealing.

Our interpretation for Spade superficially agrees with that of Rubin and Jones (2003): the meteorite was shocked, which reduced its porosity and oriented the metal grains, but some degree of annealing removed the high degree of orientation to what we see today. This annealing also resulted in some olivine recovery, possibly lessening the shock stage to the prevalent S1-S2 levels found. To account for the microcracks, it is likely that Spade was shocked again after annealing, which would have increased the porosity. That is, shocked, brought to low (e.g., <3%) porosity, annealed, and then shocked again introducing microcracks that raised the porosity to the level observed (6.6%). The second shock need not have been strong, but it could have introduced the more highly shocked (S4) material we found. Alternatively, the S4 material is what remains of grains that escaped significant recovery.

4.3.9. Queen's Mercy

The H6 chondrite Queen's Mercy has a shock stage of S3 (almost S4) but is highly heterogeneous, with olivine grain shock stages almost evenly distributed between S1 and S4 (Fig. 2l). This heterogeneity occurs on a very local scale, sometimes with different grains in the same relict chondrule varying in shock stage (e.g., between S1 and S4). This suggests spatially heterogeneous response to shock. The meteorite has coarse metal veins that grade into thinner troilite and silicate melt veins, making it clear that the coarse metal veins were produced by shock mobilization. With a porosity of only 2.5%, Queen's Mercy falls into a region of samples with atypically low porosity for an S3 shock stage (Fig. 5). When the porosity and foliation strength factor are considered together, Queen's Mercy is on the borderline of being a low-SPF chondrite (Fig. 6). We propose that Queen's Mercy was shocked to attain metal and other melt veins, foliated metal, and low porosity. High foliation and low porosity together could have been enhanced if a projectile collided a warm parent body target. However, there is no evidence for annealing following impact, so the meteorite source area may not have been deeply buried following impact. An ancient $^{40}\text{Ar}/^{39}\text{Ar}$ age of 4490 ± 30 Ma (Turner et al., 1978) suggests an early impact, but possibly the meteorite source area was excavated to a near-surface region of the parent body where cooling was relatively rapid.

4.3.10. Saint-Séverin

Saint-Séverin (LL6) is a breccia containing closely-spaced clasts enclosed in finer-grained material. We included this meteorite in our sample suite because Ashworth et al. (1977) interpreted incipient recovery of dislocations in olivine grains as indicating shock during slow cooling from high temperatures. Leroux et al. (1996) also examined microstructures in the meteorite and found evidence for an additional later and mild shock event occurring at low temperatures. Hohenberg et al. (1981) found

two $^{40}\text{Ar}/^{39}\text{Ar}$ ages for different components of the meteorite, 4420 ± 10 Ma for dark and 4383 ± 10 Ma for light lithologies.

Our observations for Saint-Séverin indicate an unusually large range in olivine shock stages, including the full spectrum ranging from S1–S6 but dominated by olivine grains showing S2 (21%), S3 (22%), and S4 (34%) characteristics (Fig. 2m). There are systematic differences between three thin sections studied, with one section (USNM 2608-2) containing mainly S1–S3 material, and two others (CML 0665-1 and -2B) containing mainly S3–S4 material. The weighted shock stage is 3.25 ($N = 247$, Table 1), much higher than the S2 shock stage assigned by Rubin (2004). Porosity and metal foliation strength values are intermediate (Fig. 6). Porosity is typical of S2–S3 chondrites but also similar to that of S4 Leedey (Fig. 5), in rough agreement with the dominant S2–S4 shock stages for olivine. However, the foliation strength better matches that of an S2 chondrite (Fig. 4a).

Taken together, these data are consistent with the idea of multiple shock events for Saint-Séverin. During these events, material that was plastically deformed to differing extents (mainly S2–S4) was intimately mixed. The last significant impact probably was a weak (S2) shock event, possibly at 4383 Ma ago, which established the overall metal foliation. A late weak shock is consistent with the interpretation of Leroux et al. (1996), but the data also can be reconciled with that of Ashworth et al. (1977), if the shock and annealing effects observed by the latter authors pertain to an earlier shock event. Our data place limits on the cumulative effects of these early shock events. They could not have been much more intense than S3–S4 without reducing the porosity to below the observed value, unless porosity was increased by subsequent shocks, for which there is minimal evidence. Further, annealing could not have been so extensive so as to anneal olivine deformation to below the commonly observed S2–S4 levels.

Available data for Saint-Séverin can be reconciled with the following complex collisional history. (1) An early strong (S3–S4) shock event, possibly at ~ 4420 Ma ago, produced compacted and deformed S3–S4 materials with limited (but possibly some) post-shock annealing. (2) Brecciation mixed materials of different shock stages and largely destroyed the metal fabric produced earlier. (3) A later weak (S2) shock, possibly at ~ 4380 Ma ago, produced weakly deformed (S2) olivine, re-established a metal foliation, and re-lithified the meteorite.

4.4. Brecciation and multiple impacts

Some chondrites we examined contain heterogeneously deformed olivine (Queen's Mercy, Holbrook, Spade, Saint-Séverin, to a lesser extent Butsura and MIL 99301). This heterogeneity could be caused by inhomogeneous deformation as a result of localized pressure–temperature excursions during shock wave passage in non-uniform rocks (Sharp and DeCarli, 2006; Bland et al., 2014), or it could be the result of brecciation, which mixed grains that were deformed in different shock events.

We suggest that both inhomogeneous deformation and brecciation were important. The extreme spatial variability of olivine deformation in the same lithic features in Queen's Mercy is best explained by local pressure excursions. Pressure–temperature excursions should be larger for more porous chondrites (Bland et al., 2014). However, among the meteorites in this study there is no obvious correlation between shock heterogeneity and porosity (Table 1), and there is no evidence that variations in porosity contributed to inhomogeneous deformation. Still, we cannot rule out a significant role for inhomogeneous deformation for various chondrites.

Brecciation seems likely for both Saint-Séverin and Spade, the former because the meteorite shows obvious clasts, and the latter because the meteorite has a bimodal distribution of olivine grain shock stages (Fig. 2n). Given that all of the chondrites we examined are highly metamorphosed (type 6) chondrites that have relatively uniform grain sizes and textures, which should minimize local variations in shock pressure, we suggest that most of the meteorites with heterogeneously deformed olivine are in fact breccias.

As previously discussed in Section 4.1, one would expect multiple shock events to have the effect of decreasing porosity. Conceivably there could be a mismatch between porosity and foliation, and between porosity and shock stage, as porosity reduction should be cumulative during repeated impact, but metal foliation and shock stage should be recording the latest strong shock (Friedrich et al., 2014a, b). It therefore might be possible for a chondrite subjected to multiple impacts to become less porous than expected for a given metal foliation or shock stage. Candidates for such a history of repeated shocks include Portales Valley, GRO 85209, Kernouvé, Estacado, Queen's Mercy, and Morrow County, all of which have low porosity for a given shock stage and metal foliation strength (Figs. 5 and 6). However, except for Queen's Mercy, these chondrites do not show evidence for large dispersions in olivine shock stages that one might expect for repeated impacts (Fig. 2).

Similarly, chondrites with younger $^{40}\text{Ar}/^{39}\text{Ar}$ ages that likely experienced a long impact history do not necessarily show large dispersions in olivine grain shock stages. Good examples are Leedey, Bruderheim, Alfanello, and Morrow County, which have relatively recent $^{40}\text{Ar}/^{39}\text{Ar}$ ages (~ 460 – 3800 Ma, Table 1) and unimodal shock stage distributions (Fig. 2). Despite likely long impact histories, the shock stages, porosities, and metal foliations of these chondrites are all consistent with having been established by the last strong shock. That is, they fit the “simple model” (Fig. 1). This implies that later strong shocks “reset” the characteristics (shock stage, porosity, metal fabric) of the rocks, without any obvious regard to earlier impact history.

If later strong shocks reset shock stages and metal foliations, what is the effect of later weak shocks? As shown by Friedrich et al. (2014b), a significantly weaker late shock is not capable of reorienting metal grains. Similarly, one would not expect overall shock stages to be re-set by a later weak shock: there is no way for plastic deformation of olivine to decrease with subsequent impacts, assuming an absence of significant heating effects during and after shock.

Thus, it would appear that only in situations in which an impact breaks apart more deformed material and incorporates less deformed material can the imprints of a later shock potentially be recorded by metal foliation and the shock stages of some grains. That is, a late weak shock event that involves brecciation can potentially destroy an earlier fabric and imprint a new one, and cause an admixture of less deformed olivine grains. The best example of this could be Saint-Séverin (Section 4.3.10).

4.5. Impacts, metamorphism, and parent body structures

There is little consensus on the role played by collisions during thermal metamorphism of chondrite parent bodies. In one extreme, collisions either did not occur or were relatively insignificant during endogenic heating, resulting in an undisturbed onion-shell structure with metamorphic grade (petrographic types) increasing towards the parent body center (Trieloff et al., 2003; Kleine et al., 2008). In the other extreme, impacts thoroughly disrupted parent bodies during internal heating, causing an extensive scrambling of metamorphic grades in a re-accreted body and leading to a warm rubble pile (Grimm, 1985; Taylor et al., 1987; Ganguly et al., 2013; Scott et al., 2014). It is also possible that localized impact cratering occurred without large-scale disruption of the overall onion shell structure (Harrison and Grimm, 2010). These early impact processes can be distinguished from later events when the parent bodies were cold. For example, it is widely believed that the L-chondrite parent body was significantly disrupted ~470 Ma ago (e.g., Swindle et al., 2014 and references therein), which could have resulted in the shock effects recorded by such meteorites as Bruderheim and Morrow County.

Results here support the idea that impacts occurred during thermal metamorphism on all three ordinary chondrite asteroidal bodies. Low-SPF chondrites in this study with Ar age determinations all have old (~4460–4530 Ma) ages, although MIL 99301 also shows evidence for a younger disturbance (Table 1). These older ages correspond to the approximate time of thermal metamorphism for ordinary chondrites (e.g., Swindle et al., 2014). Conversely, non-low-SPF chondrites in this study all have younger ages (~460–4400 Ma), although Saint-Séverin also has evidence for an older event (Table 1). Thus, the data suggest that among the meteorites in this study, low-SPF chondrites were affected by early shock events while thermal metamorphism was occurring and the parent bodies were warm, and non-low-SPF chondrites were affected by later shock events while the parent bodies were cold. However, this does not rule out the existence of other non-low-SPF chondrites that were never shocked significantly. Candidates for such chondrites are those with low shock stage and foliations and high porosities, which were not part of this study.

The data provide reasons to be cautious in constructing parent body models. For example, chronology and cooling data for two H6 chondrites we studied, Kernouvé and Estacado, have been used to evaluate onion shell cooling models for the H chondrite parent body (Trieloff et al., 2003; Kleine et al., 2008; Harrison and Grimm, 2010; Scott

et al., 2014). The low (S1) shock stage of these meteorites has been used as evidence for minimal impact disturbance (Trieloff et al., 2003), but both meteorites show evidence for annealing effects that could have reduced their shock stage, and both meteorites have low porosity values that suggest they were affected by one or more impacts. Estacado also shows appreciable metal foliation suggesting impact deformation. Caution should therefore be used when assuming these meteorites were unaffected by shock. TEM observations of Kernouvé suggest that it was never significantly shocked, but that it was mildly deformed at high temperature and cooled slowly afterwards (Ruzicka et al., 2015a). This implies that for at least this meteorite, impact during metamorphic heating may not have disturbed the overall cooling setting.

As with optical deformation of olivine, physical properties including metal foliation and porosity may not be simple to interpret. Metal shape preferred orientation may not faithfully record shock compaction if annealing can destroy fabrics. Porosity is likely to decrease with impacts, but how much will depend on the impact history (single or multiple impacts) and nature of the target (warm, cool). Porosity also can be increased by impacts if the target is relatively non-porous and cool; however the porosity would be in the form of intragranular microcracks.

TEM data can provide important details about pre- and post-shock conditions, and the extent of annealing, but are limited in spatial extent (possibly not representative for the meteorite overall if effects are spatially uneven), and can be time consuming to obtain. Cooling rate and chronological approaches are also available, but can be complicated to interpret if heating and cooling history were complex.

Thus, there is no single measurement that one can obtain that can fully constrain the interior structures of the H, L, and LL chondrite parent bodies during metamorphic heating. Multiple data types for the same meteorites, and multiple meteorites of different types, together with modeling, seem the most promising way to evaluate the relative importance and interplay between impacts and metamorphic heating.

5. CONCLUSIONS

There are two good explanations for apparently weakly shocked, low-porosity, and weakly foliated (low-SPF) chondrites: (1) post-shock annealing obliterated olivine strain and/or metal foliation in these meteorites, and (2) shock occurred under warm conditions different from other chondrites, which allowed more reduction of porosity. Both explanations may be correct. Annealing and recovery could have obliterated strain and caused a reduction in shock stage (Rubin, 2004; Ruzicka et al., 2015a), and elevated temperatures would have permitted additional compaction during deformation (Nakamura et al., 2000; Hirata et al., 2008). These features can be explained by the formation of annealed chondrites at depth directly below an impact crater on an already warm parent body. Transport to deeper or shallower portions and to different cooling environments of warm bodies could have occurred. Relying on shock stage alone, as determined by observations of petro-

graphic thin section, for cooling and shock history models of ordinary chondrites may be inadequate. More broadly, it appears that portions of the parent bodies of the H, L, and LL chondrites were initially deformed and compacted while these bodies were undergoing thermal metamorphism. Shock compaction under warm conditions may have been an important accretionary process and likely helped lithify the planetesimals.

ACKNOWLEDGMENTS

This study was supported by NASA grant NNX10AH336 (Origins program, PI AR, Co-I JF). Portions of this work were performed at GeoSoilEnviroCARS (Sector 13), Advanced Photon Source (APS), Argonne National Laboratory. GeoSoilEnviroCARS is supported by the National Science Foundation – Earth Sciences (EAR-1128799) and Department of Energy-GeoSciences (DE-FG02-94ER14466). This research used resources of the Advanced Photon Source, a U.S. Department of Energy (DOE) Office of Science User Facility operated for the DOE Office of Science by Argonne National Laboratory under Contract No. DE-AC02-06CH11357.

APPENDIX A. SUPPLEMENTARY DATA

Supplementary data associated with this article can be found, in the online version, at <http://dx.doi.org/10.1016/j.gca.2016.12.039>.

REFERENCES

- Ashworth J. R. (1981) Fine structure in H-group chondrites. *Proc. Royal Soc. Lond. A* **374**, 179–194.
- Ashworth J. R., Barber D. J., Brown G. M. and Smith J. V. (1977) Electron Microscopy of Some Stony Meteorites [and Discussion]. *Phil. Trans. Royal Soc. Lond. A* **286**, 493–506.
- Bland P. A., Collins G. S., Davison T. M., Abreu N. M., Ciesla F. J., Muxworthy A. R. and Moore J. (2014) Pressure-temperature evolution of primordial solar system solids during impact-induced compaction. *Nature Communications* **5**, 541, 10.1038.
- Bogard D., Hertz F. and Johnson P. (1987) Shock effects and argon loss in samples of the Leedeey L6 chondrite experimentally shocked to 29–70 GPa pressures. *Geochim. Cosmochim. Acta* **51**, 2035–2044.
- Cain P. M., McSween H. Y. and Woodward N. B. (1986) Structural deformation of the Leoville chondrite. *Earth Planet. Sci. Lett.* **77**, 165–175.
- Consolmagno G. J., Macke R. J., Rochette P., Britt D. T. and Gattacceca J. (2006) Density, magnetic susceptibility, and the characterization of ordinary chondrite falls and showers. *Meteorit. Planet. Sci.* **41**, 331–342.
- Consolmagno G. J., Britt D. T. and Macke R. J. (2008) The significance of meteorite density and porosity. *Chem. Erde* **68**, 1–29.
- Dixon E. T., Bogard D. D., Garrison D. H. and Rubin A. E. (2004) ^{39}Ar - ^{40}Ar evidence for early impact events on the LL parent body. *Geochim. Cosmochim. Acta* **68**, 3779–3790.
- Dyl K. A., Benedix G. K., Bland, P. A., Friedrich J. M., Spurný P., Towner M. C., O'Keefe M.-C., Howard K., Greenwood R., Macke R. J., Britt D. T., Halfpenny A., Thostenson J. O., Rudolph R. A., Rivers M. L., Bevan A. W. R. (2016) Characterization of Mason Gully (H5): The Second Recovered Fall from the Desert Fireball Network. *Meteorit. Planet. Sci.* **51**, 596–613. doi: 10.1111/maps.12605.
- Friedrich J. M. and Rivers M. L. (2013) Three-dimensional imaging of ordinary chondrite microporosity at 2.6 micrometer resolution. *Geochim. Cosmochim. Acta* **116**, 63–70. <http://dx.doi.org/10.1016/j.gca.2011.08.045>.
- Friedrich J. M., Wignarajah D. P., Chaudhary S., Rivers M. L., Nehru C. E. and Ebel D. S. (2008a) Three-dimensional petrography of metal phases in equilibrated L chondrites—Effects of shock loading and dynamic compaction. *Earth Planet. Sci. Lett.* **275**, 172–180. <http://dx.doi.org/10.1016/j.epsl.2008.08.024>.
- Friedrich J. M., Macke R. J., Wignarajah D. P., Rivers M. L., Britt D. T. and Ebel D. S. (2008b) Pore size distribution in an uncompactized equilibrated ordinary chondrite. *Planet. Space Sci.* **56**, 895–900. <http://dx.doi.org/10.1016/j.pss.2008.02.002>.
- Friedrich J. M., Ruzicka A., Rivers M. L., Ebel D. S., Thostenson J. O. and Rudolph R. A. (2013) Metal veins in the Kernouvé (H6 S1) chondrite: Evidence for pre- or syn-metamorphic shear deformation. *Geochim. Cosmochim. Acta* **116**, 71–83. <http://dx.doi.org/10.1016/j.gca.2013.01.009>.
- Friedrich J. M., Rubin A. E., Beard S. P., Swindle T. D., Isachsen C. E., Rivers M. L. and Macke R. J. (2014a) Ancient porosity preserved in ordinary chondrites: examining shock and compaction on young asteroids. *Meteorit. Planet. Sci.* **49**, 1214–1231. <http://dx.doi.org/10.1111/maps.12328>.
- Friedrich J. M., Weisberg M. K. and Rivers M. L. (2014b) Multiple impact events recorded in the NWA 7298 H chondrite breccia and the dynamical evolution of an ordinary chondrite asteroid. *Earth Planet. Sci. Lett.* **394**, 13–19. <http://dx.doi.org/10.1016/j.epsl.2014.03.016>.
- Ganguly J., Massimiliano T., Sumit C. and Kenneth D. (2013) H-chondrite parent asteroid: A multistage cooling, fragmentation and re-accretion history constrained by thermometric studies, diffusion kinetic modeling and geochronological data. *Geochim. Cosmochim. Acta* **105**, 206–220.
- Garrison D.H. and Bogard D.D. (2001) 39Ar-40Ar and space exposure ages of the unique Portales Valley H-chondrite. *Lunar Planet. Sci. Conf.* **32**, abstr. 1137.
- Gattacceca J., Rochette P., Denise M., Consolmagno G. and Folco L. (2005) An impact origin for the foliation of chondrites. *Earth Planet. Sci. Lett.* **34**, 351–368.
- Geiss J. and Hess D. C. (1958) Argon-potassium ages and the isotopic composition of argon from meteorites. *Astrophys. J.* **127**, 224–236.
- Grimm R. E. (1985) Penecontemporaneous metamorphism, fragmentation, and reassembly of ordinary chondrite parent bodies. *J. Geophys. Res.* **90**, 2022–2028.
- Guignard J. and Toplis M. J. (2015) Textural properties of iron-rich phases in H ordinary chondrites and quantitative links to the degree of thermal metamorphism. *Geochim. Cosmochim. Acta* **149**, 45–63.
- Harrison K. and Grimm R. E. (2010) Thermal constraints on the early history of the H-chondrite parent body reconsidered. *Geochim. Cosmochim. Acta* **74**, 5410–5423.
- Henke S., Gail H.-P., Trierloff M., Schwarz W. H. and Kleine T. (2012) Thermal evolution and sintering of chondritic planetesimals. *Astro. & Astrophys.* **537**, A45.
- Hirata N., Kurita K. and Sekine T. (2008) Simulation experiments for shocked primitive materials in the Solar System. *Phys. Earth Planet. Int.* **174**, 227–241.
- Hohenberg C. M., Hudon B., Kennedy B. M. and Podosek F. A. (1981) Noble gas retention chronologies for the St. Severin meteorite. *Geochim. Cosmochim. Acta* **45**, 535–540.
- Hutchison R. (2004) *Meteorites: A Petrologic*. Cambridge University Press, Cambridge, Chemical and Isotopic Synthesis.

- Jamsja N. and Ruzicka A. (2010) Shock and thermal history of Northwest Africa 4859, an annealed impact melt breccia of LL chondrite parentage containing unusual igneous features and pentlandite. *Meteorit. Planet. Sci.* **45**, 828–849.
- Jenniskens P., Rubin A. E., Yin Q.-Z., Sears D. W. G., Sandford S. A., Zolensky M. E., Krot A. N., Blair L., Kane D., Utas J., Verish R., Friedrich J. M., Wimpenny J., Eppich G. R., Ziegler K., Verosub K. L., Rowland D. J., Albers J., Gural P. S., Grigsby B., Fries M. D., Matson R., Johnston M., Silber E., Brown P., Yamakawa A., Sanborn M. E., Laubenstein M., Welton K. C., Nishiizumi K., Meier M. M. M., Busemann H., Clay P., Schmitt-Kopplin Ph., Glavin D. P., Callahan M. P., Dworkin J. P., Wu Q., Zare R. N., Grady M., Verchovsky S., Emel'yanko V., Naroenkov S., Clark D., Girten B. and Worden P. S. (2014) Fall, Recovery, and Characterization of the Novato L6 chondrite breccia. *Meteorit. Planet. Sci.* **49**, 1388–1425. <http://dx.doi.org/10.1111/maps.12323>.
- Kleine T., Touboul M., Van Orman J. A., Bourdon B., Maden C., Mezger K. and Halliday A. N. (2008) Hf-W thermochronometry: closure temperature and constraints on the accretion and cooling history of the H chondrite parent body. *Earth Planet. Sci. Lett.* **270**, 106–118.
- Kohout T., Gritsevich M., Grokhovsky V. I., Yakovlev G. A., Haloda J., Halodova P., Michallik R. M., Penttilä A. and Muinonen K. (2014) Mineralogy, reflectance spectra, and physical properties of the Chelyabinsk LL5 chondrite – Insight into shock-induced changes in asteroid regoliths. *Icarus* **228**, 78–85.
- Kring D. A., Hill D. H., Gleason J. D., Britt D. T., Consolmagno G. J., Farmer M., Wilson S. and Haag R. (1999) Portales Valley: A meteoritic sample of the brecciated and metal-veined floor of an impact crater on an H-chondrite asteroid. *Meteorit. Planet. Sci.* **34**, 663–669.
- Kunz J., Falter M. and Jessberger E. K. (1997) Shocked meteorites: argon-40-argon-39 evidence for multiple impacts. *Meteorit. Planet. Sci.* **32**, 647–670.
- Leroux H., Doukhan J.-C. and Guyot F. (1996) An analytical electron microscopy (AEM) investigation of opaque inclusions in some type 6 ordinary chondrites. *Meteorit. Planet. Sci.* **31**, 767–776.
- Macke R. J. (2010) Survey of meteorite physical properties: density, porosity, and magnetic susceptibility. Ph. D. thesis, University of Central Florida.
- Macke R. J., Kent J. J., Kiefer W. S. and Britt D. T. (2015) 3D-Laser-Scanning Technique Applied to Bulk Density Measurements of Apollo Lunar Samples. 46th Lunar and Planetary Science Conference (abstract #1716).
- Nakamura T., Tomeoka K., Sekine T. and Takeda H. (1995) Impact-induced chondrite flattening in the Allende CV3 carbonaceous chondrite: shock experiments. *Meteoritics* **30**, 344–347.
- Nakamura T., Tomeoka K., Takaoka N., Sekine T. and Takeda H. (2000) Impact-induced textural changes of CV carbonaceous chondrites: experimental reproduction. *Icarus* **146**, 289–300.
- Popova O. P., Jenniskens P., Emel'yanenko V., Kartashova A., Biryukov E., Khaibrakhmanov S., Shuvalov V., Rybnov Y., Dudorov A., Grokhovsky V. I., Badyukov D. D., Yin Q.-Z., Gural P. S., Albers J., Granvik M., Evers L. G., Kuiper J., Kharlamov V., Solovyov A., Rusakov Y. S., Korotkiy S., Serdyuk I., Korochantsev A. V., Larionov M. Yu., Glazachev D., Mayer A. E., Gisler G., Gladkovsky S. V., Wimpenny J., Sanborn M. E., Yamakawa A., Verosub K. L., Rowland D. J., Roeske S., Botto N. W., Friedrich J. M., Zolensky M. E., Le L., Ross D., Ziegler K., Nakamura T., Ahn I., Lee J. I., Zhou Q., Li Z.-H., Li Q.-L., Liu Y., Tang G.-Q., Hiroi T., Sears D., Weinstein I. A., Vokhmintsev A. S., Ishchenko A. V., Schmitt-Kopplin T., Hertkorn N., Nagao K., Haba M. K., Komatsu M. and Mikouchi T. (2013) Chelyabinsk Airburst, Damage Assessment, Meteorite Recovery and Characterization. *Science* **234**, 1069–1073. <http://dx.doi.org/10.1126/science.1242642>.
- Rubin A. E. (2002) Post-shock annealing of Miller Range 99301 (LL6): Implications for impact heating of ordinary chondrites. *Geochim. Cosmochim. Acta* **66**, 327–3337.
- Rubin A. E. (2004) Postshock annealing and postannealing shock in equilibrated ordinary chondrites: Implications for the thermal and shock histories of chondritic asteroids. *Geochim. Cosmochim. Acta* **68**, 673–689.
- Rubin A. E. and Jones R. H. (2003) Spade: An H chondrite impact-melt breccia that experienced post-shock annealing. *Meteorit. Planet. Sci.* **38**, 1507–1520.
- Ruzicka A., Killgore M., Mittlefehldt D. W. and Fries M. D. (2005) Portales Valley: Petrology of a metallic melt meteorite breccia. *Meteorit. Planet. Sci.* **40**, 261–295.
- Ruzicka A., Hugo R. and Hutson M. (2015a) Deformation and thermal histories of ordinary chondrites: Evidence for post-deformation annealing and syn-metamorphic shock. *Geochim. Cosmochim. Acta* **163**, 219–233.
- Ruzicka A.M., Clay P.M., Hugo R., Joy K.H. and Busemann H. (2015b) Contrasting early and late shock effects on the L chondrite parent body: Evidence from Ar ages and olivine microstructures for two meteorites. *Meteorit. Planet. Sci.*, Abstract #5177.
- Sasso M. R., Macke R. J., Boesenberg J. S., Britt D. T., Rivers M. L., Ebel D. S. and Friedrich J. M. (2009) Incompletely compacted equilibrated ordinary chondrites. *Meteorit. Planet. Sci.* **44**, 1743–1753. <http://dx.doi.org/10.1111/j.1945-5100.2009.tb01204.x>.
- Schmitt R. T. (2000) Shock experiments with the H6 chondrite Kernouve: Pressure calibration of microscopic shock effects. *Meteorit. Planet. Sci.* **35**, 545–560.
- Scott E. R. D., Krot T. V., Goldstein J. I. and Wakita S. (2014) Thermal and impact history of the H chondrite parent asteroid during metamorphism: Constraints from metallic Fe–Ni. *Geochim. Cosmochim. Acta* **136**, 13–37.
- Sharp T. G. and DeCarli P. S. (2006) Shock Effects in Meteorites. In *Meteorites and the Early Solar System II* (eds. D. S. Lauretta and J. H. Y. McSween). University of Arizona Press, Tucson, pp. 653–677.
- Sneyd D. S., McSween, Jr., H. Y., Sugiura N., Strangway D. W. and Nord, Jr., G. L. (1988) Origin of petrofabrics and magnetic anisotropy in ordinary chondrites. *Meteoritics* **23**, 139–149.
- Stöfler D., Keil K. and Scott E. R. D. (1991) Shock metamorphism of ordinary chondrites. *Geochim. Cosmochim. Acta* **55**, 3845–3867.
- Swindle T. D., Kring D. A. and Weirich J. R. (2014) $^{40}\text{Ar}/^{39}\text{Ar}$ ages of impacts involving ordinary chondrite meteorites. *Geological Society, London, Special Publications* **378**, 333–347.
- Taylor G. J., Maggiore P., Scott E. R. D., Rubin A. E. and Keil K. (1987) Original structures, and fragmentation and reassembly histories of asteroids - Evidence from meteorites. *Icarus* **69**, 1–13.
- Trieloff M., Jessberger E. K., Herrwerth I., Hopp J., Fiéni C., Ghélis M., Bourot-Denise M. and Pellas P. (2003) Structure and thermal history of the H-chondrite parent asteroid revealed by thermochronometry. *Earth Planet. Sci. Lett.* **190**, 267–269.
- Turner G. (1969) Thermal histories of meteorites by the ^{39}Ar – ^{40}Ar method. In *Meteorite Research. D* (ed. P. Millman). Reidel, Dordrecht, pp. 407–417.
- Turner G., Miller J. A. and Grasty R. L. (1966) The thermal history of the Bruderheim meteorite. *Earth Planet. Sci. Lett.* **1**, 155–157.

Turner G., Enright M.C. and Cadogan P.H. (1978) The early history of chondrite parent bodies inferred from ^{40}Ar – ^{39}Ar ages. Proc. Lunar Planet. Sci. Conf. 9th, 989–1025.

Woodcock N. H. (1977) Specification of fabric shapes using an eigenvalue method. *Geo. Soc. Am. Bull.* **88**, 1231–1236.

Woodcock N. H. and Naylor M. A. (1983) Randomness testing in three-dimensional orientation data. *J. Struct. Geo.* **5**, 539–548.

Associate editor: Pierre Beck